Research Article

Azzh Saad Alshehry, Humaira Yasmin*, and Rasool Shah

3D thin-film nanofluid flow with heat transfer on an inclined disc by using HWCM

https://doi.org/10.1515/phys-2023-0122
received August 02, 2023; accepted October 02, 2023

Abstract: Momentum and heat transmission influence the coated physical characteristics of wire product. As a result, understanding the polymeric movement and heat mass distribution is crucial. An increase in thermal efficiency is necessary for the wire covering technology. So, the aim of this work is to investigate the influence of nanomaterials on the heat and mass transport processes in wire coating analyses. A thin film nanofluid is used to investigate heat and mass transfer in three dimensions over a rotating inclined disc. Both the suction and injection effects of nanofluids and the thermal radiation of their fluxes are taken into account. By employing similarity variables, the set of governing equations can be transformed into a differential equation system. The necessary differential equation system is solved using the Haar wavelet collocation method. Plots and observations of the velocity distribution, concentration, and thermal fields within the boundary layer across an inclining, steadily rotating plane are made. Flow characteristics change as a result of varying embedded factors such as S, Sc, N_b, Pr, and thermophoretic parameters. Evidence suggests that as the number of rotation parameters grows, the thermal boundary layer weakens.

Keywords: Haar wavelet collocation method, thermal radiation, heat production/consumption, nanofluid, spinning disc, thin film flow

1 Introduction

In order to generate the nonlinear differential equation, a similarity transformation was applied to the original fluid flow model. A set of differential equation system is derived from these equations. The first-order differential equations have been converted into a set of fractional differential equations with the help of the Haar wavelet collocation method (HWCM) [1–3].

The removal of saturated vapor from a fluid condensate during cooling is an important step in the development of chemical and mechanical engineering. Many researchers have replicated this issue under varying situations. Nanoparticle deferrals in fluids exhibit substantial endowment enhancement at low nanoparticle concentrations. Nanofluids have been the subject of extensive study because of the critical importance of direct heat transfer enrichment in various manufacturing applications, transportation systems, and nuclear power plants [4,5]. It has also been detailed how nanofluid can be used as a “smart fluid” in which heat transfer can be controlled to increase or decrease as needed. This study’s overarching objective is to have a conversation about the myriad ways in which nanofluids are currently being and will be used in the future, with a focus on the enhanced heat transfer properties that can be regulated and the specific characteristics that these nanofluids keep [6,7]. Chemical and applied sciences rely heavily on solving the problem of liquid condensation from cool, saturated vapors. Several studies have examined this phenomenon under different frameworks.

Adding nanoparticles to regular fluids improves their thermal performance significantly. Bhatti *et al.* [8] studied the simultaneous effects of a changing magnetic field on Jeffrey nanofluid. Ellahi [9] considered the flow of a magnetohydrodynamic (MHD) non-Newtonian nanofluid whose viscosity changes with temperature. Hatami and Ganji [10] investigated nanofluid laminar flow between rotating discs with heat transfer, using the microchannel heat sink as a cooling medium and the least square method and porous media approach as cooling mechanisms, respectively. Throughout the extant literature, the common fluid is predominantly used as a

*** Corresponding author: Humaira Yasmin,** Department of Basic Sciences, Preparatory Year Deanship, King Faisal University, Al-Ahsa, 31982, Saudi Arabia, e-mail: hhassain@kfu.edu.sa
Azzh Saad Alshehry: Department of Mathematical Sciences, Faculty of Sciences, Princess Nourah Bint Abdulrahman University, P.O. Box 84428, Riyadh 11671, Saudi Arabia
Rasool Shah: Department of Mathematics, Abdul Wali Khan University, Mardan, Pakistan

low-thermal-conductivity base fluid. The outputs of these thermal systems are incredibly modest. Improving fluid thermal activity by dispersing microscopic particles called nanoparticles throughout the fluid. Sheikholeslami *et al.* [11] studied the fluid flow over an inclined plane.

There are numerous practical uses for studying time-dependent fluid flow in engineering and other scientific disciplines. Attia [12] studied flow on a disc using suction and injection. In their research, Bachok *et al.* [13] analyzed the fluid dynamics of a moving porous plate. With the use of nanofluids, they were able to improve heat transfer. Freidoonimehr *et al.* [14] analyzed numerically the streaming of a nanoliquid across porous expanding media. Makinde *et al.* [15] looked into the effect of varying viscosity on the streaming of a nanoliquid. Akbar *et al.* [16] analyzed the 2D stream of a nanoliquid by employing a magnetic field, and numerical results were derived by a shooting method. The MHD stream of a nanoliquid produced by a rotating disc was investigated by Ramzan *et al.* [17] under partial slip conditions. Recent studies [18–23] provide a comprehensive investigation of nanofluid streaming with various properties.

In the polymerization industry, wire coating is typically used as an insulating substance and protection against mechanical damage. This method involves pulling and submerging an exposed, warmed wire into the melting polymer [24,25]. During this procedure, the heated polymer is also extruded across a rolling wire. Because of its widespread application in science, technology, and engineering, thin-film flow research has recently come to the forefront. Non-viscous flow has real-world applications, such as in developing cables, wires, fibber coats, *etc*. Sandeep and Malvandi [26] investigated the thin-film fluid flow of non-Newtonian nanoliquids . According to Wang's [27] measurements, there is a variation in the thin-film fluid's flow through the stretching sheet. Usha and Sridharan [28] analyzed unstable finite thin liquid as it moves past a straight surface. Liu and Andersson [29] discussed the film flow with heat on a surface. Aziz *et al.* [30] imagined fluid moving as a thin layer on a stretching sheet to generate internal heat. Tawade *et al.* [31] analyzed thin film thermal radiation and convection. A thorough investigation of thermal radiations can be further enhanced by referring to the comprehensive analysis provided in previous scholarly publications [32–38] and the diverse investigations encompassed within them. Andersona *et al.* [39] pondered fluid film flow on a stretching sheet with heat transfer. Moreover, researchers [40–43] have considered the irregular motion of liquid films on a stretching surface to account for additional variations. Hatami *et al.* [44] used a steadily spinning disc to study the movement of nanofluids in three dimensions.

Considering the foregoing extensive discussion, this study seeks to examine the flow of nanofluid for cooling purposes in the wire surface coatings.

2 Mathematical formulation

Consider the flow of a nanofluid thin layer in three dimensions over a spinning disc that is deemed a wire. As can be seen in Figure 1, the rate at which the disc spins in its own plane, expressed as an angular velocity, is given by Ω. The slanted disc is at an inclination of degree β with respect to the horizontal plane. Here, h represents the nanofluid layer thickness and V_w represents the spraying velocity. Since the liquid sheet is so thin in relation to the disc's radius, the cumulative effect can be disregarded. As expected, the downward force of gravity (acceleration denoted by the symbol g) is in effect. The film surface temperature is denoted by the letter T_s, while the disc surface temperature is denoted by T_d. A similar C_s concentration is found on a

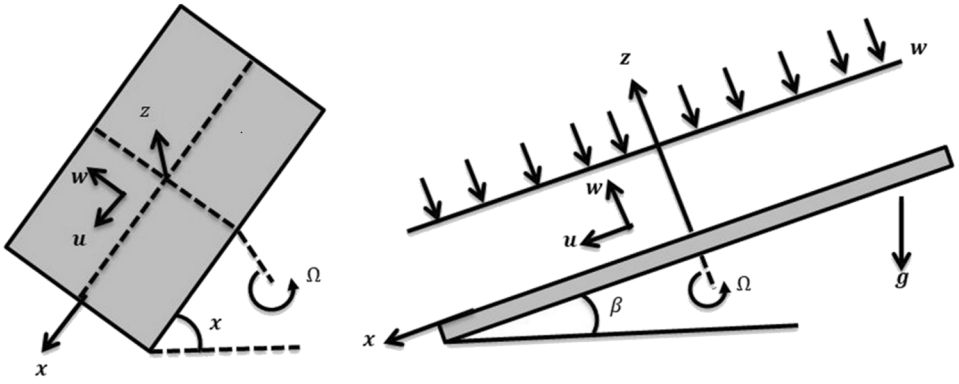

Figure 1: Schematic diagram.

film's surface, while a C_d concentration is found on the disc. By maintaining a fixed value for $p_\circ$ at the film's surface, the pressure is reduced to a simple function of the z-axis.

The basic flow equations are given as follows:

$$\nabla.\ \vec{u} = 0, \tag{1}$$

$$\rho\left[u\frac{\partial u}{\partial x} + v\frac{\partial u}{\partial y} + w\frac{\partial u}{\partial z} + \frac{\partial u}{\partial t}\right] = \mu\left[\frac{\partial^2 u}{\partial x^2} + \frac{\partial^2 u}{\partial y^2} + \frac{\partial^2 u}{\partial z^2}\right] + \rho g\sin\beta, \tag{2}$$

$$\rho\left[u\frac{\partial u}{\partial x} + v\frac{\partial u}{\partial y} + w\frac{\partial u}{\partial z} + \frac{\partial v}{\partial t}\right] = \mu\left[\frac{\partial^2 v}{\partial x^2} + \frac{\partial^2 v}{\partial y^2} + \frac{\partial^2 v}{\partial z^2}\right], \tag{3}$$

$$\rho\left[u\frac{\partial u}{\partial x} + v\frac{\partial u}{\partial y} + w\frac{\partial u}{\partial z} + \frac{\partial w}{\partial t}\right] = \mu\left[\frac{\partial^2 w}{\partial x^2} + \frac{\partial^2 w}{\partial y^2} + \frac{\partial^2 w}{\partial z^2}\right] + \rho g\cos\beta - p_z, \tag{4}$$

$$\left([uvw]\nabla.\ T + \frac{\partial T}{\partial t}\right) = \alpha(\nabla^2.\ T) - \left[\frac{(\rho c_p)_p}{(\rho c_p)_f}\right] \times \left[D_b\left(\frac{\partial C}{\partial x}\frac{\partial T}{\partial x} + \frac{\partial C}{\partial y}\frac{\partial T}{\partial y} + \frac{\partial C}{\partial z}\frac{\partial T}{\partial z}\right) + \frac{Dt}{T}\left\{\left(\frac{\partial T}{\partial x}\right)^2 + \left(\frac{\partial T}{\partial y}\right)^2 + \left(\frac{\partial T}{\partial z}\right)^2\right\}\right], \tag{5}$$

$$\left[u\frac{\partial C}{\partial x} + v\frac{\partial C}{\partial y} + w\frac{\partial C}{\partial z} + \frac{\partial C}{\partial t}\right] = D_b(\nabla^2 C) + \frac{Dt}{T_\circ}\left(\frac{\partial^2 T}{\partial x^2} + \frac{\partial^2 T}{\partial y^2} + \frac{\partial^2 T}{\partial z^2}\right). \tag{6}$$

With boundary conditions,

$$\begin{aligned} &u = -\Omega_x, v = -\Omega_y, w = 0, T = T_s, C = C_s, \text{ at } z = 0,\\ &u_z = 0, v_z = 0, w = -W, T = T_\circ, C = C_\circ, p = p_\circ, \text{ at}\\ &z = h. \end{aligned} \tag{7}$$

Let us consider the following non-dimensionalized parameters:

$$\begin{aligned} u &= \frac{-\Omega_x}{1-b_t}g + \frac{\Omega_x}{1-b_t}f' + g(-bt+1)^{-\frac{1}{2}}k\sin\frac{\beta}{\Omega},\\ v &= -\Omega_y(-bt+1)^{-\frac{1}{2}}g + \Omega_y(-bt+1)^{-\frac{1}{2}}f'\\ &\quad + (-bt+1)^{-\frac{1}{2}}gh\sin\frac{\beta}{\Omega}, \end{aligned} \tag{8}$$

$$w = -2\sqrt{\frac{\Omega v_f}{1-b_t}}f,\ \eta\theta = \frac{T-T_d}{T_\circ - T_d},\ \eta\phi = \frac{C-C_d}{C_\circ - C_d},\ \eta = z\sqrt{\frac{\Omega}{v_f(1-b_t)}}. \tag{9}$$

With the help of the above defined parameters, one can obtain the governing non-dimensionalized equations:

$$D^3 f - (Df)^2 + g^2 - 2fD^2 f - S\left(Df + \frac{\eta D^2 f}{2}\right) = 0, \tag{10}$$

$$D^2 K - KD(f) - h(\eta)g(\eta) + 2fD(K) + 1 - \frac{S(K + \eta D(K))}{2} = 0, \tag{11}$$

$$D^2 g - 2gD(f) + 2D(g)f - S\left(D(g) + \frac{\eta D(g)}{2}\right) = 0, \tag{12}$$

$$D^2 h - K(\eta)g(\eta) - hD(f) + 2fD(h) - \frac{S(h - \eta D(h))}{2} = 0, \tag{13}$$

$$D^2\theta + 2\mathrm{Pr}fD(\theta) + N_b\theta'\phi' + N_t(\theta')^2 + \frac{S(\eta\theta' + \eta^2\theta'')}{2} = 0, \tag{14}$$

$$D^2(\phi) + 2ScfD(\phi) + \frac{N_t}{N_b}\theta'' + \frac{S(\eta\phi' + \eta^2\phi'')}{2} = 0. \tag{15}$$

With boundary conditions,

$$\begin{aligned} f(0) = Df(0) = 0, D^2 f_\delta = g(0) = 0, Dg_\delta = K(0)\\ = D(K)_\delta = 0, h(0) = \theta(0) = D(h)_\delta = \phi(0)\\ = 0, \theta(\delta) = \phi(\delta) = 1, \end{aligned} \tag{16}$$

where the parameters Pr, Sc, N_b, N_t, and S are defined as follows:

$$\mathrm{Pr} = \frac{\mu}{\rho_f},\ \mathrm{Sc} = \frac{\mu}{\rho_f D},\ N_b = \frac{(\rho c)_p D_b C_h}{(\rho c)_f},\ N_t = \frac{(\rho c)_p D_t T_h}{(\rho c)_f T_s},\ S = \frac{\alpha}{\Omega}, \tag{17}$$

$$\delta = \varepsilon\sqrt{\frac{\Omega}{v_f(1-bt)}},\ f(\delta) = \frac{w}{2\sqrt{\Omega v}},\ \theta' = \frac{1}{\delta}. \tag{18}$$

The equation $\delta = \varepsilon\sqrt{\frac{\Omega}{v_f(1-bt)}}$ yields the constant normalized thickness. The phenomenon under consideration is understood by means of the condensation or spraying velocity, denoted as $f(\delta) = \frac{w}{2\sqrt{v\,\Omega}} = \alpha$. The pressure can be determined using the process of integrating Eq. (4). For Pr = 0 and $\theta(\delta) = 1$, the exact solution is represented by

$$\theta'(0) = \frac{1}{\delta}. \tag{19}$$

The equation $\delta = \varepsilon\sqrt{\frac{\Omega}{v_f(1-bt)}}$ represents the asymptotic limit for a small (δ). The non-monotonic nature of the decline of $\theta'(0)$ with increasing (δ) can be observed from the oscillatory behavior of the curves for large (Pr):

$$N_u = \frac{\left(\frac{\partial T}{\partial z}\right)}{T_o - T_d} = \delta\theta'(0). \tag{20}$$

In the same way, the Sherwood number is defined as follows:

$$S_h = \frac{\left(\frac{\partial C}{\partial z}\right)}{C_o - C_d} = \delta\theta'(0). \tag{21}$$

3 Methodology

Assume that A and B are constants, then for $x \in [A, B]$, the definition of the ith Haar wavelet family is

$$H_i(x) = \begin{cases} 1 & \text{for} \quad x \in [a_1, b_1) \\ -1 & \text{for} \quad x \in [b_1, c_1) \\ 0 & \text{elsewhere} \end{cases}, \tag{22}$$

$$a_1 = \frac{k}{m_1}, b_1 = \frac{k + \frac{1}{2}}{m_1}, c_1 = \frac{k+1}{m_1}, \tag{23}$$

where $m_1 = 2^j$ is the highest attainable resolution, we will refer to this quantity as $M = 2j$, and each of the $2M$ subintervals of the interval $[A, B]$ has length $x = (B, A)/2M$, where M is the number of subintervals $(2M)$. A translation parameter $k = 0,1,\ldots, m_1 - 1$ and a dilatation parameter $j = 0,1,\ldots, J$. The formula for the wavelet number i is $i = m_1 + k + 1$.

For the Haar function and its integrals

$$p_{i1}(x) = \int_0^x H_i(x'), \tag{24}$$

$$p_{i,l+1}(x) = \int_0^x p_{i,l}(x')\mathrm{d}x', \; l = 1, 2 \ldots \tag{25}$$

In order to calculate these integrals, we use Eq. (22)

$$p_{i1}(x) = \begin{cases} x - a_1 & \text{for} \quad x \in [a_1, b_1) \\ c_1 - x & \text{for} \quad x \in [b_1, c_1) \\ 0 & \text{elsewhere} \end{cases}, \tag{26}$$

$$p_{i2}(x) = \begin{cases} \frac{1}{2}(x - a_1)^2 & \text{for} \quad x \in [a_1, b_1) \\ \frac{1}{4m_1^2} - \frac{1}{2}(c_1 - x)^2 & \text{for} \quad x \in [b_1, c_1) \\ \frac{1}{4m_1^2} & \text{for} \quad x \in [c_1, 1) \\ 0 & \text{elsewhere} \end{cases}, \tag{27}$$

$$p_{i3}(x) = \begin{cases} \frac{1}{6}(x - a_1)^3 & \text{for} \quad x \in [a_1, b_1) \\ \frac{1}{4m_1^2}(x - b_1) - \frac{1}{6}(c_1 - x)^3 & \text{for} \quad x \in [b_1, c_1) \\ \frac{1}{4m_1^2}(x - \beta) & \text{for} \quad x \in [c_1, 1) \\ 0 & \text{elsewhere} \end{cases}. \tag{28}$$

We also present the notation shown below:

$$C_{i1} = \int_0^L p_{i1}(x')\mathrm{d}x', \tag{29}$$

$$C_{i2} = \int_0^L H_i(x')\mathrm{d}x'. \tag{30}$$

Summation of the Haar wavelet function can be written as follows:

$$f(x) = \sum_{i=1}^{\infty} a_i H_i(x). \tag{31}$$

Using wavelets, we may approximate the highest order derivatives of $f, \theta, g, h, K,$ and ϕ given by problems (10)–(14) and (15) to build a straightforward and precise HWCM

$$f'''(\eta) = \sum_{i=1}^{2M} a_i H_i(\eta), \tag{32}$$

$$g''(\eta) = \sum_{i=1}^{2M} b_i H_i(\eta), \tag{33}$$

$$\theta''(\eta) = \sum_{i=1}^{2M} c_i H_i(\eta), \tag{34}$$

$$\phi''(\eta) = \sum_{i=1}^{2M} d_i H_i(\eta), \tag{35}$$

$$h''(\eta) = \sum_{i=1}^{2M} e_i H_i(\eta), \tag{36}$$

$$K''(\eta) = \sum_{i=1}^{2M} f_i H_i(\eta). \tag{37}$$

Integrating Eq. (32), we obtain the values $f'''(\eta)$, $f''(\eta), f'(\eta)$, and $f(\eta)$, respectively,

$$f'''(\eta) = \sum_{i=1}^{2M} a_i \left(p_{i,1}(\eta) - \frac{1}{L} C_{i,1} \right), \tag{38}$$

$$f''(\eta) = \sum_{i=1}^{2M} a_i \left(p_{i,2}(\eta) - \frac{1}{L} \eta C_{i,1} \right), \tag{39}$$

$$f'(\eta) = \sum_{i=1}^{2M} a_i \left(p_{i,3}(\eta) - \frac{1}{L} \frac{\eta^2}{2} C_{i,1} \right), \tag{40}$$

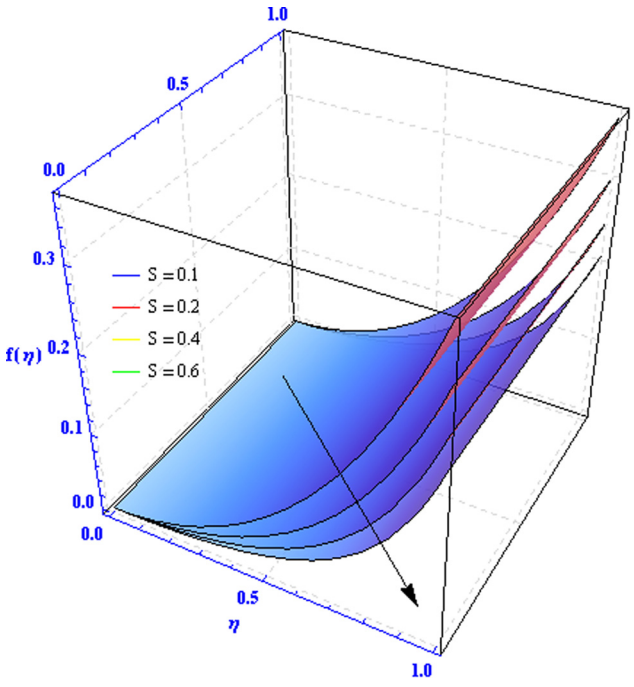

Figure 2: Variation of "S" on $f(\eta)$ for $N_b = N_t = Sc = 0.5$, $Pr = 6.7$.

$$f(\eta) = \sum_{i=1}^{2M} a_i \left(p_{i,4}(\eta) - \frac{1}{L} \frac{\eta^3}{3} C_{i,1} \right). \tag{41}$$

Assume L is a large number. The numerical solution for the given system is obtained by substituting Eqs (32)–(41) into Eqs (10)–(15). In the next section, we see a visual representation of the results of the proposed solution.

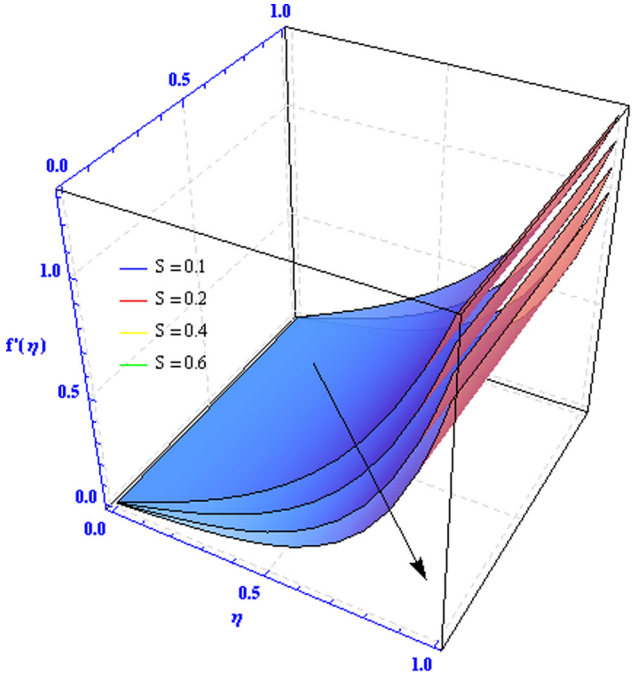

Figure 3: Variation of "S" on $f'(\eta)$ for $N_b = N_t = Sc = 0.5$, $Pr = 6.7$.

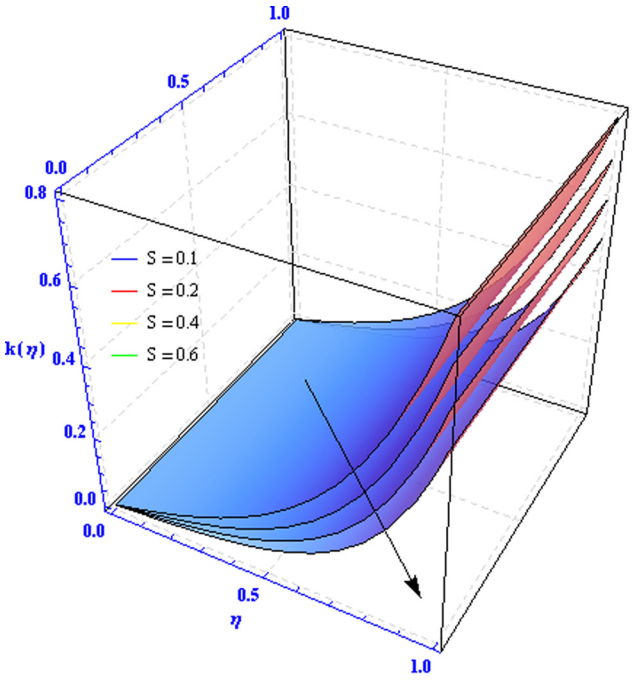

Figure 4: Variation of "S" on $k(\eta)$ for $N_b = N_t = Sc = 0.5$, $Pr = 6.7$.

4 Results and discussion

This study investigates fluid flow characteristics in thin-film nanofluids within a three-dimensional framework. Specifically, we examine the behavior of these nanofluids

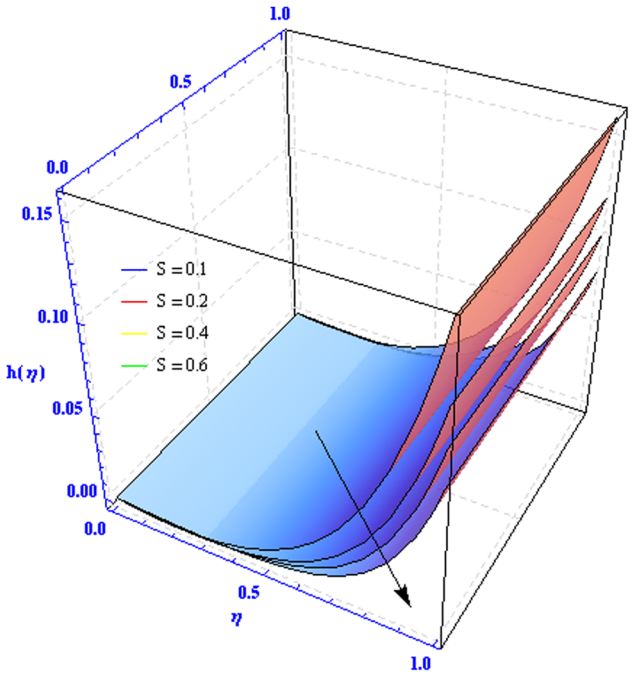

Figure 5: Variation of "S" on $h(\eta)$ for $N_b = N_t = Sc = 0.5$, $Pr = 6.7$.

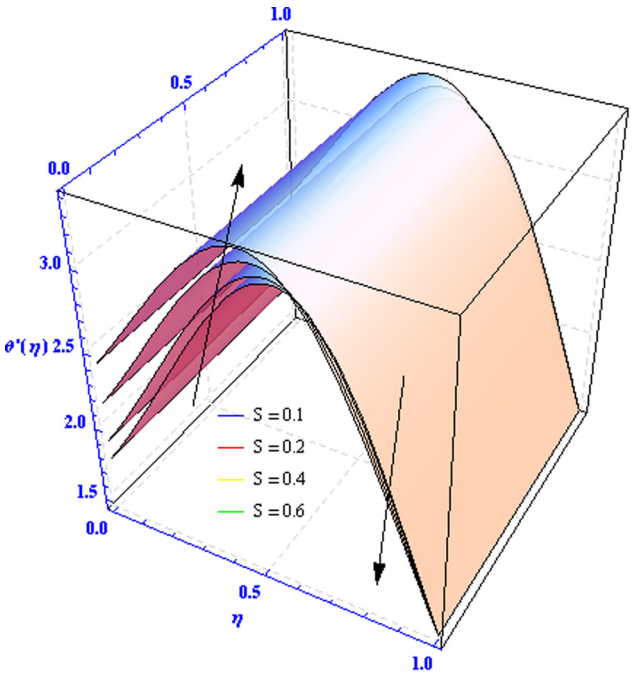

Figure 6: Variation of "S" on θ' for $N_b = N_t$ = Sc = 0.5, Pr = 6.7.

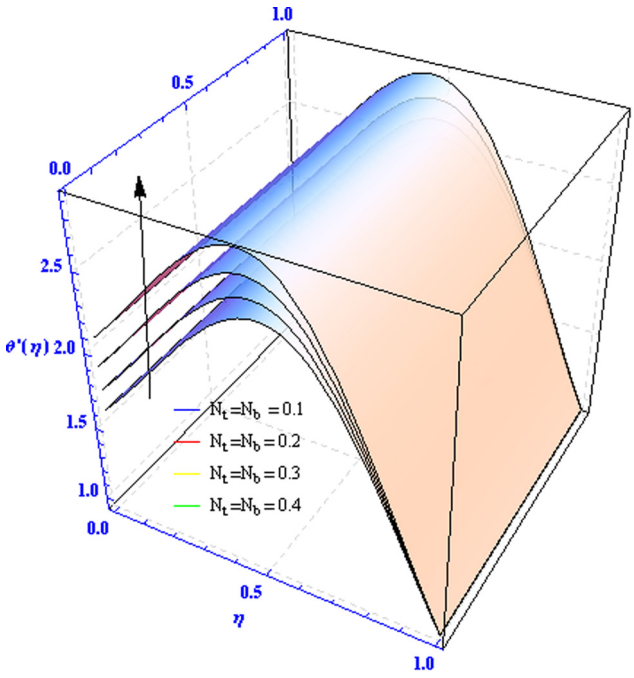

Figure 8: Variation of "N_t, N_b" on $\theta'(\eta)$ for S = Sc = 0.5, Pr = 6.7.

across an inclined and rotating surface, with a particular emphasis on the associated heat and mass transfer processes. The focus of our work has been to analyze the impact of different embedded characteristics. The findings were achieved using the HWCM. Figure 1 depicts the schematic state of the flow. Variations in the value of the parameter (S) and their effects on the axial velocity, radial velocity, drainage flow, and induced flow are depicted in Figures 2–5. Higher values of the parameter (S) signify more significant fluctuations in the fluid velocity. This effect is considerably obvious and it holds true for all of

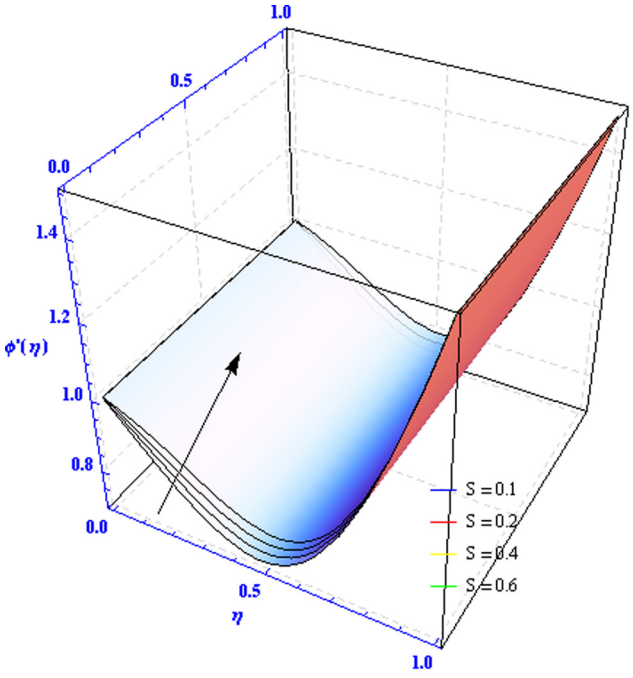

Figure 7: Variation of "S" on $\phi'(\eta)$ for $N_b = N_t$ = Sc = 0.5, Pr = 6.7.

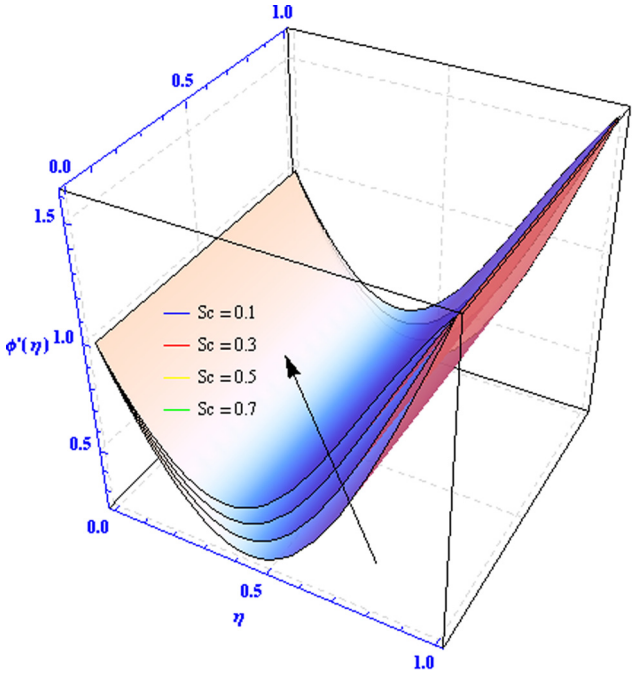

Figure 9: Variation of "Sc" on $\phi'(\eta)$ for $S = N_t = N_p$ = 0.5, Pr = 6.7.

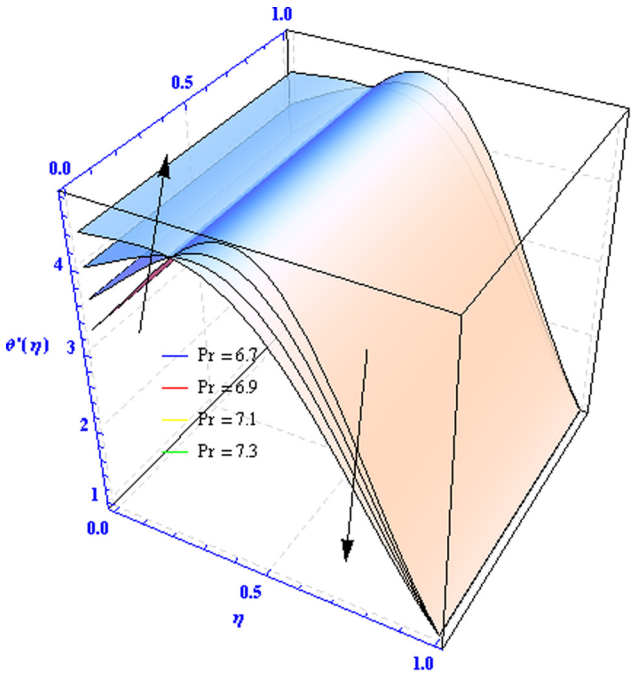

Figure 10: Variation of "P_r" on $\theta'(\eta)$ for Sc = N_t = N_b = 0.5.

the aforementioned different types of fluid motion that emerge with greater values of (S), as the thickness of the momentum barrier layer increases. This result is modified in Figure 6, where the temperature profiles continue to fall as (S) increases. In reality, increasing the amount of S cools the system and slows down the rate at which heat is transferred from the sheet to the fluid. Molecular collisions within the fluid are slowed down physically but only slightly.

As illustrated in Figure 7, the concentration profile rises as the unsteadiness parameter (S) is increased. This is because a thicker momentum boundary layer results in a higher concentration profile. The point-wise rate of change inherent in this situation makes this effect more efficient and transparent.

As can be seen in Figure 8, the heat transfer rate improves with increasing values of (N_t) and (N_b). As can be seen in Figure 9, the concentration rate rises as (Sc) (Schmidt number) is changed. Actually, the kinematic viscosity increases as (Sc) grows larger, and the Sherwood

Table 1: Numerical solution of the HWC approach Sc = S = 0.5, Pr = 6.7, N_t = N_b = 0.5

η	$f(\eta)$	$f'(\eta)$	$\theta'(\eta)$	$k(\eta)$	$\phi'(\eta)$	$h(\eta)$
0	0.012222	0.002136	1.11918	0.001021	0.013215	0.092328
0.1	0.016141	0.0594279	1.30172	0.164447	0.059058	0.096225
0.2	0.219794	0.136644	1.41946	0.309963	0.109512	0.010135
0.3	0.249326	0.228574	1.56612	0.437877	1.152476	0.010774
0.4	0.280665	0.331357	1.93674	0.550058	1.188817	0.011539
0.5	0.290019	0.441102	2.27418	0.648589	1.219154	0.124272
0.6	0.323463	0.55441	2.35061	0.735506	1.243934	0.139431
0.7	0.357075	0.6686	3.57273	0.812652	1.263408	0.149434
0.8	0.370967	0.781725	3.92233	0.851608	1.277633	0.154355
0.9	0.395266	0.992468	4.01623	0.843696	1.286467	0.155058
1	0.402134	1.387695	4.05592	0.897643	1.589538	0.158441

Table 2: Analytical (HAM) and numerical approach (HWCM) to evaluating the function $f(\eta)$ and $f'(\eta)$ are compared
Sc = S = 0.5, Pr = 6.7, N_t = N_b = 0.5

(η)	HWCM calculations		Ham calculations		Absolute error	
0.0	0.012222	0.002136	0.012223	0.002136	0.000001	4.873421×10^{-8}
0.1	0.016141	0.059427	0.016141	0.059427	4.573421×10^{-8}	5.743610×10^{-8}
0.2	0.219794	0.136644	0.219794	0.136645	3.973421×10^{-7}	−0.000001
0.3	0.249326	0.228574	0.249327	0.228574	0.000002	3.457235×10^{-8}
0.4	0.280665	0.331357	0.280665	0.331289	4.172121×10^{-9}	0.000068
0.5	0.290019	0.441102	0.290017	0.441102	0.000002	4.842367×10^{-6}
0.6	0.323463	0.554410	0.323463	0.554395	6.873421×10^{-7}	0.000015
0.7	0.357075	0.668656	0.357076	0.668653	0.000030	0.000026
0.8	0.370967	0.781725	0.370967	0.781725	2.871121×10^{-6}	6.845295×10^{-8}
0.9	0.395266	0.992468	0.395267	0.992466	0.000005	0.000002
1	0.402134	1.387695	0.402133	1.387694	0.000001	0.000135

Table 3: Analytical (HAM) and numerical approach (HWCM) to evaluating the function $\theta'(\eta)$ and $k(\eta)$ are compared
Sc = S = 0.5, Pr = 6.7, $N_t = N_b = 0.5$

(η)	HWCM calculations		Ham calculations		Absolute error	
0.0	1.11918	0.001021	1.11910	0.001021	0.000080	0.000000
0.1	1.30172	0.164447	1.30145	0.164442	0.000270	0.000005
0.2	1.41946	0.309963	1.41923	0.309961	0.000230	0.000002
0.3	1.56612	0.437877	1.56612	0.437871	2.172121×10^{-9}	0.000006
0.4	1.93674	0.550058	1.93670	0.550058	0.000040	4.198120×10^{-5}
0.5	2.27418	0.648589	2.27418	0.648586	4.172021×10^{-7}	0.000003
0.6	2.35061	0.735506	2.35056	0.735500	0.000050	0.000006
0.7	3.57273	0.812652	3.57273	0.812651	6.170121×10^{-8}	0.000001
0.8	3.92233	0.851608	3.92223	0.851603	0.000100	0.000005
0.9	4.01623	0.843696	4.01589	0.843689	0.000340	0.000007
1	4.05592	0.897643	4.05591	0.897638	0.000010	0.000005

Table 4: Analytical (HAM) and numerical approach (HWCM) to evaluating the function $\phi(\eta)$ and $h(\eta)$ are compared
Sc = S = 0.5, Pr = 6.7, $N_t = N_b = 0.5$

(η)	HWCM calculations		Ham calculations		Absolute error	
0.0	0.013215	0.092328	0.013215	0.092328	3.173464×10^{-8}	5.174321×10^{-8}
0.1	0.059058	0.096225	0.059036	0.096219	0.000022	0.000007
0.2	0.109512	0.010135	0.109506	0.010130	0.000006	0.000005
0.3	1.152476	0.010774	1.152465	0.010773	0.000011	0.000002
0.4	1.188817	0.011539	1.188815	0.011537	0.000002	0.000003
0.5	1.219154	0.124272	1.219145	0.124270	0.000009	0.000002
0.6	1.243934	0.139431	1.243933	0.139430	0.000001	0.000001
0.7	1.263408	0.149434	1.263407	0.149428	0.000001	0.000006
0.8	1.277633	0.154355	1.277628	0.154346	0.000005	0.000010
0.9	1.286467	0.155058	1.286458	0.155045	0.000009	0.000013
1	1.589538	0.158441	1.589529	0.158389	0.000009	0.000053

number decreases with the increase in concentration of the chemical species.

Figure 10 depicts the relationship between the Prandtl number (Pr) and the heat transfer rate. When the Prandtl number increases, the thermal boundary layer thins out, slowing the rate at which the system cools. In the initial stages, this impact takes on a quite distinct form. This is because there is a ceiling on the effect caused by the pointwise rate of change.

The numerical results of the HWCM are presented in Table 1. The study incorporates a comprehensive analysis utilizing numerical and analytical HAM calculations. The findings are shown in Tables 2–4, providing a complete comparison between the two methods. The data indicate a significant level of concurrence between the HAM and numerical results, suggesting a strong level of precision in our conclusions. The investigation demonstrates a minimal absolute error between our numerical results and the calculations based on the HAM. Therefore, it is apparent that our numerical computations are in complete agreement with the analytical HAM outcomes.

5 Conclusion

This study focuses on examining the complexities of the dynamics of three-dimensional nanofluid spraying over a spinning inclined disc, which is similar to the wire utilized in practical surface coating applications. The following discussion summarizes the novel findings discovered in the current investigation.

As the unsteadiness parameter (S) increases, the temperature field decreases due to the increase of the momentum barrier layer's thickness.

An increase in the Schmidt number (Sc) leads to a decrease in the Sherwood number as a result of an

increase in the kinematic viscosity and concentration of the chemical species.

With larger values of the Prandtl number (Pr), the Nusselt number decreases. Although the initial effect is very different, as the value decreases, we notice an increase in boundary layer flow turbulence.

Increasing the proportion of nanofluids in the system, the temperature profile decreases, and the lowest temperature is reached.

The velocity profile declines for parameter S due to the internal collision of the small fluid particles.

Acknowledgments: Princess Nourah bint Abdulrahman University Researchers Supporting Project number (PNURSP2023R183), Princess Nourah bint Abdulrahman University, Riyadh, Saudi Arabia. Thiswork was supported by the Deanship of Scientific Research, the Vice Presidency for Graduate Studiesand Scientific Research, King Faisal University, Saudi Arabia (Grant No. 4383).

Funding information: This work was supported by Princess Nourah bint Abdulrahman University Researchers SupportingProject number (PNURSP2023R183), Princess Nourah bint Abdulrahman University, Riyadh, SaudiArabia. This work was supported by the Deanship of Scientific Research, the Vice Presidency forGraduate Studies and Scientific Research, King Faisal University, Saudi Arabia (Grant No. 4383).

Author contributions: All authors have accepted responsibility for the entire content of this manuscript and approved its submission.

Conflict of interest: The authors state no conflict of interest.

References

[1] Lepik U. Haar wavelet method for nonlinear integro- differential equations. Appl Math Comput. 2006;176:324–33.

[2] Lepik U. Numerical solution of evolution equations by the Haar wavelet method. Appl Math Comput. 2007;185:695–704.

[3] Siraj-ul-Islam, Sarler B, Aziz I, Haq F. Haar wavelet collocation method for the numerical solution of boundary layer fluid flow problems. Therm Sci. 2011;50:686–97.

[4] Yasmin H, Giwa SO, Noor S, Sharifpur M. Experimental exploration of hybrid nanofluids as energy-efficient fluids in solar and thermal energy storage applications. Nanomaterials. 2023;13:278.

[5] Yasmin H, Giwa SO, Noor S, Sharifpur M. Thermal conductivity enhancement of metal oxide nanofluids: A critical review. Nanomaterials. 2023;13:597.

[6] Nisar Z, Yasmin H. Analysis of motile gyrotactic micro-organisms for the bioconvection peristaltic flow of carreau–yasuda bionanomaterials. Coatings. 2023;13:314.

[7] Yasmin H, Giwa SO, Noor S, Aybar HS. Reproduction of nanofluid synthesis, thermal properties and experiments in engineering: A research paradigm shift. Energies. 2023;16:1145.

[8] Bhatti MM, Zeeshan A, Ellahi R. Simultaneous effects of coagulation and variable magnetic field on peristaltically induced motion of Jeffrey nanofluid containing gyrotactic microorganism. Microvasc Res. 2017;110:32–42.

[9] Ellahi R. The effects of MHD and temperature dependent viscosity on the flow of non-Newtonian nanofluid in a pipe: analytical solutions. Appl Math Model. 2013;37:1451–67.

[10] Hatami M, Ganji DD. Thermal and flow analysis of microchannel heat sink (MCHS) cooled by Cu-water nanofluid using porous media approach and least square method. Energ Convers Manage. 2014;78:347–58.

[11] Sheikholeslami M, Hatami M, Ganji DD. Numerical investigation of nanofluid spraying on an inclined rotating disk for cooling process. J Mol Liq. 2015;211:577–83.

[12] Attia HA. Unsteady MHD flow near a rotating porous disk with uniform suction or injection. Fluid Dyn Res. 1998;23:283.

[13] Bachok N, Ishak A, Pop I. Unsteady boundary-layer flow and heat transfer of a nanofluid over a permeable stretching/shrinking sheet. Int J Heat Mass Transf. 2012;55:2102–9.

[14] Freidoonimehr N, Rashidi MM, Mahmud S. Unsteady MHD free convective flow past a permeable stretching vertical surface in a nano-fluid. Int J Therm Sci. 2015;87:136–45.

[15] Makinde OD, Mabood F, Khan WA, Tshehla MS. MHD flow of a variable viscosity nanofluid over a radially stretching convective surface with radiative heat. J Mol Liq. 2016;219:624–30.

[16] Akbar T, Batool S, Nawaz R, Zia QMZ. Magnetohydrodynamics flow of nanofluid due to stretching/shrinking surface with slip effect. Adv Mech Eng. 2017;9:1.

[17] Ramzan M, Chung JD, Ullah N. Partial slip effect in the flow of MHD micropolar nanofluid flow due to a rotating disk-A numerical approach. Results Phys. 2017;7:3557–66.

[18] Al-Rashed AA, Kalidasan K, Kolsi L, Aydi A, Malekshah EH, Hussein AK, et al. Three-dimensional investigation of the effects of external magnetic field inclination on laminar natural convection heat transfer in CNT–water nanofluid filled cavity. J Mol Liq. 2018;252:454–68.

[19] Alshomrani AS, Gul T. A convective study of Al_2O_3-H_2O and Cu-H_2O nano-liquid films sprayed over a stretching cylinder with viscous dissipation. Eur Phys J Plus. 2017;132:495.

[20] Gul T, Firdous K. The experimental study to examine the stable dispersion of the graphene nanoparticles and to look at the GO-H_2O nanofluid flow between two rotating disks. Appl Nanosci. 2018;8:1711–27.

[21] Demir Y, Işleyen SK. Evaluation of mathematical models for flexible job-shop scheduling problems. Appl Math Model. 2013 Feb;37(3):977–88.

[22] Ellahi R, Zeeshan A, Waheed A, Shehzad N, Sait SM. Natural convection nanofluid flow with heat transfer analysis of carbon nanotubes–water nanofluid inside a vertical truncated wavy cone. Math Methods Appl Sci. 2023 Jul;46(10):11303–21.

[23] Khan AA, Arshad A, Ellahi R, Sait SM. Heat transmission in Darcy-Forchheimer flow of Sutterby nanofluid containing gyrotactic microorganisms. Int J Numer Methods Heat Fluid Flow. 2023 Jan;33(1):135–52.

[24] Khan Z, Khan I, Ahammad NA, Basha DB, Andualem M. Effect of nanoparticles on wire surface coating using viscoelastic third-grade fluid as a coating polymer inside permeable covering die with variable viscosity and magnetic field. J Nanomaterials. 2022;2022:1111657.
[25] Ali F, Zahid M, Hou Y, Manafian J, Rana MA, Hajar A. A theoretical study of reverse roll coating for a non-isothermal third-grade fluid under lubrication approximation theory. Math Probl Eng. 2022;2022:5029132.
[26] Sandeep N, Malvandi A. Enhanced heat transfer in liquid thin film flow of non-Newtonian nanofluids embedded with graphene nanoparticles. Adv Powder Technol. 2016;27:2448–56.
[27] Wang CY. Liquid film on an unsteady stretching surface. Q Appl Math. 1990;84:601–10.
[28] Usha R, Sridharan R. On the motion of a liquid film on an unsteady stretching surface. ASME Fluids Eng. 1993;150:43–8.
[29] Liu IC, Andersson IH. Heat transfer in a liquid film on an unsteady stretching sheet. Int J Therm Sci. 2008;47:766–72.
[30] Aziz RC, Hashim I, Alomari AK. Thin film flow and heat transfer on an unsteady stretching sheet with internal heating. Meccanica. 2011;46:349–57.
[31] Metri PG, Tawade J, Abel MS. Thin film flow and heat transfer over an unsteady stretching sheet with thermal radiation internal heating in presence of external magnetic field. Int J Adv Appl Math Mech. 2016;3:29–40.
[32] Ezzat MA, El-Karamany AS, El-Bary AA, Fayik MA. Fractional calculus in one-dimensional isotropic thermo-viscoelasticity. C R Méc. 2013;341:553–66.
[33] Ezzat MA, El-Karamany AS, El-Bary AA. On thermo-viscoelasticity with variable thermal conductivity and fractional-order heat transfer. Int J Thermophys. 2015;36(7):1684–97.
[34] Ezzat MA, El-Bary AA, Morsey MM. Space approach to the hydro-magnetic flow of a dusty fluid through a porous medium. Comput Math Appl. 2010;59:2868–79.
[35] Ezzat M, El-Bary AA, Ezzat S. Combined heat and mass Transfer for unsteady MHD flow of perfect conducting. Energy Convers Manag. 2011;52:934–45.
[36] Yasein MD, Mabrouk N, Lotfy K, El-Bary AA. The influence of variable thermal conductivity of semiconductor elastic medium during photothermal excitation subjected to thermal ramp type. Results Phys. 2019;25(12):4731–40.
[37] Ezzat MA, El-Bary AA. Effects of variable thermal conductivity on Stokes' flow of a thermoelectric fluid with fractional order of heat transfer. Int J Therm Sci. 2016;100:305–15.
[38] El-Bary AA. Hyperbolic two-temperature generalized thermoelasticity with fractional order strain of solid cylinder. J Eng Therm Sci. 2021 Dec;1(2)):30–42.
[39] Anderssona HI, Aarseth JB, Dandapatb BS. Heat transfer in a liquid film on an unsteady stretching. Int J Heat Mass Transf. 2000;43:69–74.
[40] Chen CH. Heat transfer in a power-law liquid film over an unsteady stretching sheet. Heat Mass Transf. 2003;39:791–6.
[41] Chen CH. Effect of viscous dissipation on heat transfer in a non-Newtonian liquid film over an unsteady stretching sheet. J Non-Newton Fluid. 2006;135:128–35.
[42] Wang C, Pop L. Analysis of the flow of a power-law liquid film on an unsteady stretching surface by means of homotopy analysis method. J Non-Newton Fluid. 2006;138:161–72.
[43] Mahmoud MAA. On flow and heat transfer in a thin liquid film over an unsteady stretching sheet with variable fluid properties and radiation. Open Sci J Math Appl. 2015;3:14–8.
[44] Hatami M, Jing D, Majeed AY. Three-dimensional analysis of condensation nanofluid film on an inclined rotating disk by efficient analytical methods. Arab J Basic Appl Sci. 2018;25:28–37.